The Effect of Precracking History on Branch Crack Threshold under Mixed Mode I/II loading.

R. A. Baloch M. W. Brown
UNIVERSITY OF SHEFFIELD, U K

Third International Conference on Biaxial/Multiaxial Fatigue,
April 3 - 6 1989, Stuttgart F R G

1 ABSTRACT

The effect of mode I fatigue precracking surfaces on branch crack threshold is studied in AISI 316 austenitic stainless steel at room temperature under mode II and mixed mode I/II loading. A branch crack is formed at higher stress intensities when a large number of crack growth increments are introduced near threshold during precracking. It is suggested that because of crack surface roughness interactions, the crack driving force at the precrack tip($\Delta K_{Ieff}, \Delta K_{IIeff}$) was less than the nominal value.

A method for estimating the effective stress intensity factors ΔK_{Ieff} and ΔK_{IIeff} is proposed and the branch crack threshold is predicted by a local stress intensity factor criterion. Scanning Electron Microscopy analysis of precrack surfaces showed damaged surfaces due to surface roughness interactions.

NOMENCLATURE

a	crack length
a_o	initial crack length
a_b	branch crack length
B	specimen thickness
A m	material constants
eff	effective
h_i	space between potential drop leads
K_I, K_{II}	stress intensity factors for mode I and II
M	bending moment
N_f	number of cycles to failure
PD	potential drop
P	applied load
Q	shear force
R	load ratio $\frac{P_{min}}{P_{max}}$
S	span distance
th	threshold
W	specimen width
Y	specimen geometry
Δ	as prefix, range of stress or K
Δa	a-a_o
θ_m	measured branch angle
θ_c	calculated branch angle
U	closure ratio $\frac{K_{eff}}{K_I}$
V_i	PD across the crack for leads at spacing h_i

2 Introduction

In fracture mechanics, there are three fundamental modes by which fatigue crack extension can occour, shown in Fig. 1, being (i) the opening mode, where crack surfaces move directly apart, (ii) the edge sliding mode, where crack surfaces slide over each other in a direction perpendicular to the leading edge of the crack, and (iii) the tearing mode, where crack surfaces also slide with respect to each other but parallel to the leading edge. In linear elastic fracture mechanics (LEFM) situations the crack tip stress fields can be described in the terms of three stress intensity factors (K_I, K_{II}, K_{III}). Near the threshold for fatigue crack propagation (FCP), complex crystallograpic mechanisms for crack extension occur (1). But at higher stress intensities, the FCP rate can be characterised by the well known Paris equation (2) for mode I propagation,

$$\frac{da}{dN} = A\,(\Delta K)^m \tag{1}$$

where

$$\Delta K = Y\,\Delta\sigma_{eff}\,\sqrt{\pi a}, \tag{2}$$

where $\Delta\sigma_{eff}$ is the stress range for which the crack is open during a cycle.

The fatigue crack growth threshold range, ΔK_{th} is an important parameter, in the determination of the safety of structures. Threshold can be defined as the value of the mode I stress intensity factor range ΔK_{th} below which a fatigue crack remains dormant or grows very slowly at an experimentally undetectable speed (1). A large amount of research work has concentrated on mode I models dealing with relationships between FCP rate, stress intensity factor range, and the threshold condition for fatigue crack growth. However pure mode I loading does not always exist, when fabrication defects or cracks in structures and components are not normal to the maximum principal stress or when tensile and torsional loads are simultaneously applied. These defects lead to mixed mode cracking.

The growth of fatigue cracks under mixed mode loading was first studied by Iida and Kobayashi(3). They examined fatigue crack growth in aluminium plates under cyclic tensile loads, where the initial crack was inclined to the tensile axis. Under cyclic load, a branch crack was formed in the direction perpendicular to the loading axis where ΔK_I was maximum. Since then many mixed mode FCP results have been published. Some examples are given below.

Pook and Greenan (4) used the Jones and Chisholm(5) specimens (an edge sliding mode compact specimen) to study fatigue crack growth in En3 mild steel. The specimens were precracked in fatigue under mode I loading, and then fatigue tests were conducted under mode II loading at R=0.048. The results were plotted as an "S-N curve", i.e N_f as a function of K_{II}. The endurance limit of precracked specimens was defined as the threshold, ΔK_{IIth}. They reported that in all cases, crack growth was at an angle of roughly 70° to the precrack. For some specimens the branch crack initiated at the end of the machined slot, but for others branch crack was initiated at the precrack tip. For specimens with long precracks the branch crack was formed on the precrack flank some distance behind the tip.

Otsuka et al (6,7) studied the threshold behaviour of low carbon steel with two grain sizes, structural steel and an aluminium alloy under fully reversed (R = -1) mode II with

superimposed static mode I loading. Instead of forming a branch, coplanar crystallographic growth was observed in the low carbon steel at low stress intensities. With static mode I loading superimposed the coplanar cracks did not arrest, as observed by Gao et al.(8), but little acceleration in crack growth rate was observed. It remained constant at 10^{-7} mm/cycle, until a branch crack was formed at higher stress intensities. No coplanar growth was observed in structural steel as a branch crack was formed immediately. In aluminium alloy at threshold mode I branch cracking was observed, but by applying a higher load continuous mode II growth was observed with a higher growth rate than for the branched mode I.

Gao et al (8) examined mixed mode threshold behaviour in AISI 316 stainless steel using beam specimens with combined bending and shear loading. They observed a very limited amount of coplanar growth from the spark machined slit when no fatigue precracking was employed. However in precracked specimens, crystallographic coplanar crack growth was observed, but the cracks became non-propagating. Not until branching at higher stress intensities did the cracks grow to failure.

Smith (9) examined the effects of crack surface interaction on growth of fatigue cracks under mode II loading in a structural steel. He reported that crack surface interaction was dominant, the effective stress intensity was much less than the nominally applied value e.g. (ΔK_{IIeff}= 0.5 xΔK_{II} at ΔK_{II}= 19 MN$m^{\frac{-3}{2}}$ R=0.05) and that a mode I branch crack was formed after a short amount of coplanar growth. When static mode I loading was superimposed, the crack surface interaction was reduced so that the threshold of mode I branching was less than the value predicted by the maximum tangential stress criterion using nominal mode I threshold.

In the present paper the effect of prior fatigue cracking surfaces on mode II and mixed mode I and II loading is studied in AISI 316 stainless steel at room temperature for linear elastic plane strain conditions. Different $\frac{\Delta K_{II}}{\Delta K_I}$ ratios and fixed R ratios of 0.1 and 0.5 were employed to investigate the effect of fracture surfaces on branch crack threshold. The results obtained are discussed and the branch crack threshold is predicted by using a local stress intensity criterion.The fracture surfaces were examined with a Scanning Electron Microscope.

3 Material and Test Procedure

All the tests were completed on AISI 316 austenitic stainless steel plate, solution treated and water quenched. The rolling direction was parallel to the longitudinal axis of the specimens. The average austenite grain size was 40μm.The chemical composition and mechanical properties are shown in Table 1. The same specimen geometry used by Gao et al(8) was used. For pure mode I three point bending was employed whereas for mode II and mixed mode I/II loading asymmetric four point bend specimens were used throughout this work.
For pure mode I the crack tip stress intensity factor was calculated using the formula given in ASTM-E-399-83 (10), valid for all a/W,

$$K_I = \frac{P\,S}{4\,B\,W^{\frac{3}{2}}}\,f(\frac{a}{W}) \qquad (3)$$

where

$$f(\frac{a}{W}) = \frac{6\,(\frac{a}{W})^{\frac{1}{2}}\left\{1.99-(\frac{a}{W})(1-\frac{a}{W})(2.15-3.93(\frac{a}{W})+2.7(\frac{a}{W})^2)\right\}}{(1+2(\frac{a}{W}))(1-(\frac{a}{W}))^{\frac{3}{2}}} \quad (4)$$

For mixed mode I/II loading, a four point asymmetric bending arrangement with the crack plane displaced from the plane of symmetry was used, as shown in Fig. 2. The crack tip stress intensity factors K_I and K_{II} were calculated by numerical methods for a straight crack by Wang et al.(11), and tabulated and used by Gao et al.(8). However in this report the results of Bentham and Koiter (12) for mode I in pure bending, f_b, were used with Wang's equation (11) for mode II cracks,

$$f_s = \frac{1}{f_b}\int_0^x (f_b)^2 dx \quad (5)$$

which was numerically integrated to obtain the following K calibration for mixed mode loading. For the mode I component

$$K_I = \frac{M}{B\,W^{\frac{3}{2}}} f_b(\frac{a}{W}) \quad (6)$$

where

$$f_b = 6\left\{\pi(\frac{a}{W})\right\}^{\frac{1}{2}}\left\{1.12-1.39(\frac{a}{W})+7.32(\frac{a}{W})^2-13.1(\frac{a}{W})^3+14.0(\frac{a}{W})^4\right\} \quad (7)$$

after Brown and Srawley (13), and for the mode II component,

$$K_{II} = \frac{Q}{B\,W^{\frac{1}{2}}} f_s(\frac{a}{W}) \quad (8)$$

where

$$f_s = \left\{\pi(\frac{a}{W})\right\}^{\frac{1}{2}}\left\{3.3645(\frac{a}{W})-1.051(\frac{a}{W})^2-0.526(\frac{a}{W})^3+1.89(\frac{a}{W})^4\right\} \quad (9)$$

For equations (7) and (9) to be valid, two conditions must be obeyed (11),

(i) $0 < \frac{a}{W} < 0.6$ (ii) $\frac{(S_1-S_o)}{W} > \frac{2}{3}$

To ensure that linear elastic plane strain conditions were satisfied and boundary effects were small, all the specimen dimensions B, a, (W-a), S_1 and S_2 were at least fifty times greater than the crack tip monotonic plastic zone size. The average shear stress on the uncracked ligament was less than 50% of the shear yield stress, which itself was taken as half of the 0.2% offset tensile yield strength of the material.

4 Experimental Procedure

All the tests were carried out on a Mayes servo hydraulic fatigue machine incorporating a bending fixture. The machine was operated under load control, with a sinusoidal waveform of frequency 20 Hz to 80 Hz. The crack length was measured by using a travelling microscope and the D.C. potential drop (PD) method simultaneously. A crack growth increment of 0.04mm at 30X magnification could be resolved. The PD exhibited a better

sensitivity than the microscope, specially when the crack grew at mid thickness of the specimen. A constant current of 30 amps was passed through the specimen. The leads for measurement of the PD were made from 316 stainless steel, spot welded onto the specimen. The position of four leads is shown in Fig.3. A change in the voltage ratio $\frac{V_1}{V_2}$ of 0.043 corresponded to 0.1 mm crack extension for straight crack of length 15 mm. The straight crack length can be derived from a pair of simultaneous equations given by the Gilbey and Pearson formula (14), after eliminating the unknown K,

$$cos(\frac{\pi a}{2\ W}) = A_1\ sech(K\ V_1) \tag{10}$$

$$cos(\frac{\pi a}{2\ W}) = A_2\ sech(K\ V_2) \tag{11}$$

where constants A_1 and A_2 are determined by fitting two measured crack lengths, being the initial and the final values for the test.

4.1 Precracking down to threshold

Some specimens were fatigue precracked down to threshold under mode I conditions by using three point symmetric bending. The crack was initiated from a slit produced by spark erosion. A stress intensity factor range ΔK higher than ΔK_{th} was applied to produce a fatigue crack.This was followed by periodically decreasing the maximum load in 10% increments. At each step the crack was allowed to grow a distance of several times the previous plastic zone size to minimize the effect of residual stresses. Precracking was ceased when no crack extension could be detected after $6x10^5$cycles, indicating less than $8x10^{-8}$mm/cycle growth rate.

4.2 Precracking at Constant Load

Three specimens were fatigue precracked at constant load. A higher load range was applied than threshold and the crack was allowed to grow to a certain length. The detailed history of precracking is given in Tables 2 and 3 for each specimen. Specimens B5, B6 and A10 were precracked at constant load, giving the increasing ranges of stress intensity in Table 2.

5 Results

The thresholds, ΔK_{thI}, of fatigue precracked specimens were determined by the load decreasing technique. The threshold values ΔK_{thI}, for each test under R = 0.1 and R = 0.5 are listed in Tables 2 and 3 respectively. For R = 0.1 the average mode I threshold value was 4.95 $MNm^{\frac{-3}{2}}$ and for was 4.94 $MNm^{\frac{-3}{2}}$ for R = 0.5.

The results for mixed mode threshold conditions using the load increasing sequence with fixed $\frac{\Delta K_{II}}{\Delta K_I}$ and R ratio are listed Tables 4 and 5. Three distinct types of behaviour are identified, initial coplanar growth, non-propagating cracks, and formation of a branch crack. In Fig. 4 it can be seen that coplanar growth from the precrack tip is a mixed mode growth, for which a crack initiation threshold can be measured when crack extension is first detected. However such coplanar cracks are quickly arrested, and both at threshold and at higher stress levels, cracks become non-propagating after a small crack

extension Δa. At a higher stress level, the crack will branch, at an angle θ_m , and may then propagate to fracture.

In Figs. 5 and 6 the lower bound curves show the initiation of coplanar growth and the upper bound curves indicate the formation of a branch crack. It can be seen in Fig. 5 that the branch crack for precracked specimens with large crystallographic crack surfaces was formed at high stress intensities, whereas for specimens precracked at constant load the branch crack was formed at lower stress intensities. Below the lower bound curve no crack growth was observed, but when the load was increased to such a level that the stress intensity factors reached the upper bound curve a branch crack was formed, which generally grew stably to failure. However in tests B7 and B8 a branch crack continued for short distance and then stopped growing. Not until the load was increased, could these cracks accelerate towards failure. Between upper and lower bound curve in some specimens at certain load levels non-propagating coplanar cracks were observed, as listed in Tables 4 and 5. In all the specimens the precrack front was not straight, some were curved and others angular. But no correlation was found between precrack front and branch formation.

6 Discussion

For R=0.1, the branch crack was formed at low stress intensities in the specimens precracked at constant load, compared to specimens which were precracked down to threshold using a large number of increments near threshold. In two specimens B1 and B2 the branch crack was formed at rather low stress intensities, because the extent of the crystallographic crack surfaces was smaller than for the other specimens precracked down to threshold. For R=0.5, all specimens were precracked down to threshold with a large number of crack increments near threshold, so the branch crack was formed at higher stress intensities.

In mode I there are three main theories of crack closure (15):
(i) oxide induced crack closure is promoted by rough fracture surfaces, which at low ΔK value promote the formation of fretting debris between mating surfaces. The presence of oxides in a crack can reduce the effecive stress intensity for both modes I and II.
(ii) roughness induced crack closure can arise at threshold stress intensities due to the rough nature of fracture surfaces, since the plastic zone size at threshold crack growth rate is equal to the grain size of the material. Here single shear growth occurs at the crack tip, and fracture surfaces are crystallographic, or generally faceted.
(iii) plasticity induced closure in plane stress is considered to arise from lack of constraint in the wake of a crack. Behind the crack tip, material elements permanently stretched within prior plastic zones lead to interference between mating crack surfaces.

The specimens for R=0.1 and 0.5, precracked down to threshold with a large amount of crystallographic cracking, all exhibited the higher branch threshold. But those specimens for R=0.1, precracked at constant load, formed the branch crack at low stress intensities. It appears that in the former case the crack driving force (ΔK_{Ieff} and ΔK_{IIeff}) at the main crack tip was less than the nominal applied stress intensities (ΔK_I and ΔK_{II}), due to rubbing and sliding of crystallographic crack surfaces under mode II or mixed mode I/II loading.

However no satisfactory criterion for the formation of branch cracks appears to exist. The branch crack could be formed when local effective stress intensity factor for an incipient branch crack reaches a critical value, ΔK_{Ith} (16). By considering this criterion to be valid branch crack threshold curves in Fig. 5 and 6 were predicted by calculating a local stress intensity factor Δk_I as a function of ΔK_{Ieff} and ΔK_{IIeff} for the main crack and θ_c direction. It was supposed that the crack surface roughness-interaction under mixed mode loading may occur from the start of crystallographic surfaces up to the precrack tip. However crystallographic surfaces under mode I loading commence where the plastic zone size is equal to the grain size of the material (15), during precracking. Therefore the amount of crystallographic crack surface d_{ac} was estimated from Tables 2 and 3 by reference to the pure mode I plastic zone size,

$$r_p = \frac{1}{6\pi}\left\{\frac{\Delta K}{\sigma_{ys}}\right\}^2 \tag{12}$$

where ΔK is stress intensity factor range and σ_{ys} is yield stress of the material. The extent of cracking for $r_p < 40\mu$m was determined from Tables 2 and 3 to give d_{ac}.
The local stress intensity factor for a branch crack was calculated by the maximum tangential stress criterion (17) and used by Pook (16),

$$\Delta k_{Ieff} = cos\,\frac{\theta_c}{2}\left\{\Delta K_{Ieff}\,cos^2\frac{\theta_c}{2} - \frac{3}{2}\,\Delta K_{IIeff}\,sin\,\theta_c\right\} \tag{13}$$

where k_{Ieff} is the local stress intensity factor for a branch crack, and θ_c is the branch crack direction given by

$$\Delta K_{Ieff}\,sin\theta_c + \Delta K_{IIeff}(3\,cos\theta_c - 1) = 0 \tag{14}$$

for branching in the direction of maximum tangential stress.

In equation (12) the terms ΔK_{Ieff} and ΔK_{IIeff} were calculated from U_I, U_{II}, ΔK_I, ΔK_{II}, where

$$\Delta K_{Ieff} = U_I \Delta K_I \tag{15}$$

$$\Delta K_{IIeff} = U_{II} \Delta K_{II} \tag{16}$$

$$U_I = 1 - \frac{d_{ac}}{dB}\left\{\frac{\Delta K_{II}}{\Delta K_{II} + F\,\Delta K_I}\right\}^{\frac{1}{4}} \tag{17}$$

$$U_{II} = 1 - \frac{d_{ac}}{dA}\left\{\frac{\Delta K_{II}}{\Delta K_{II} + F\,\Delta K_I}\right\}^{\frac{1}{4}} \tag{18}$$

Here d is the grain size, *dac* is the amount of crystallographic crack surfaces, A, B, F are constants with values 140, 280, 0.02 respectively, by fitting the experimental data. As the threshold values for mode I for R=0.1 and 0.5 were nearly the same (4.95 and 4.94 $MNm^{\frac{-3}{2}}$), this was presumed to be the effective threshold value. The results are correlated in Fig.7, for all tests with precracking down to threshold. Here ΔK_{Ieff} and ΔK_{IIeff} were normalised with ΔK_{Ith} and showed good agreement with theory, i.e

$$\Delta k_{Ieff} = \Delta K_{Ith} \tag{19}$$

No attempt was made to include data for precracking at constant load, in view of the unknown residual stresses remaining after precracking.

7 Fractography

Detailed fractographic analysis using a scanning electron microscope (SEM) showed that the specimens precracked down to threshold contained damaged fracture surface regions just behind the precrack tip. Examination of specimen B8 in the SEM revealed this surface damage with evidence of rubbing on mating crack surfaces behind the crack tip, see Fig. 8(i) and (ii). Where mode II coplanar growth was seen , some sign of erosion in the mode II coplanar growth was observed, as in Fig. 8 (iii). In specimen B6 (precracked at constant load) no sign of rubbing or damage was seen,Fig. 9. These observations are consistent with the fracture surface rubbing predicted in the Discussion above.

8 CONCLUSION

Near threshold fatigue crack propagation behaviour in Type 316 stainless steel was studied under mixed mode I/II loading conditions. The results obtained depend heavily on the method employed to produce a fatigue precrack, prior to mixed mode loading.

In plane strain conditions, branch cracks formed at high stress intensities for the specimens precracked down to threshold with a large number of increments near threshold. It is suggested that because of rubbing and sliding of precrack surfaces under mode II and mixed mode I/II loading, the true crack driving force at precrack tip (ΔK_{Ieff}andΔK_{IIeff}) was related to a critical value, i.e ΔK_{th}.

The values of ΔK_{Ieff} and ΔK_{IIeff} for the main crack are estimated and the branch crack threshold is predicted by a local stress intensity factor criterion. Scanning electron microscopic analysis of precrack surfaces showed damaged precrack surfaces due to surface-roughness interaction.

9 Acknowledgements

A grateful acknowledgement is presented to Dr. E. R de los Rios, for his help in fractography. Thanks are also due to the Ministry of Science and Technology, Government of Pakistan and Pakistan Space and Upper Atmosphere Research Commission for their financial support and to the Electric Power Research Institute for providing material.

This research project forms the part of collaborative programme on mixed mode fatigue, sponsored by the European Group on Fracture.

10 References

(1) Ritchie,R.O.(1979) Near threshold fatigue crack propagation in steels, Metal Reviews .24,205-230

(2) Paris,P.C. and Erdogan,F.(1963) A critical analysis of crack propagation laws, J. of Basic Engng. Trans. ASME, 85D, 528-534

(3) Iida,S.and Kobayashi,A.S.(1969) Crack propagation rate in 7075-T6 plates under cyclic tensile and transverse shear loading. J. Basic Engng. Trans. ASME, 91D, 764-769

(4) Pook,L.P. and Greenan A.F. (1976) Various aspects of fatigue crack growth, Int. Conf.

Fatigue Testing and Design, Society of Environmental Engineers, vol.2, 30.1-30.3
(5) Jones, D. L. and Chisholm, D. B., (1975) An investigation of the edge- sliding mode in fracture mechanics, Engng. Fract. Mech. 7(2), 261-276.
(6) Otsuka,A. Mori,K. Ohshima,T. and Tsuyama, S. (1980) Mode II fatigue crack propagation in alluminium alloys and mild steel, Proceedings of the 5th International Conference on Fracture, Cannes, 4, 1851-1858
(7)Otsuka,A. Mori,K. Ohshima,T. and Tsuyama, S. (1980) Fatigue crack growth of steel and aluminium alloy specimens under mode II loading, Journal of the Society of Material Science, Japan, 29, 1042-1048
(8) Gao Hua, Brown,M.W and Miller,K.J.(1982) Mixed mode fatigue threshold. Fatigue of Engng. Mat. and Struct. 5, No.1. 1-17
(9) Smith, M. C. (1984) Some aspects of mode II fatigue crack growth, Ph.D Thesis, University of Cambridge.
(10) ASTM standards E399-83, Standard test method for plane strain fracture toughness of metallic materials, Appendix 3.
(11) Wang, K.J., Hsu, C.L and Kao, H.(1977) Calculation of stress intensity factors for combined mode bend specimens. Proceedings of the 4th International Conference on Fracture, 4, 123-133. Pergamon Press.
(12) Bentham, J.P. and Koiter, W.T. (1972) Asymptotic approximation to crack problems. Ed. G.C. Sih, Noordhof International Publishing.
(13) Brown, W.F. and Srawley, J.E. (1966) Plane strain crack toughness testing of high strength metallic materials. ASTM STP 410.
(14) Gilbey, D.M. and Pearson, S. (1966) Measurement of the length of a central crack and edge crack in a sheet of metal by an electrical resistance method. Royal Aircraft Establishment Technical Report 66402.
(15) Suresh, S. and Ritchie, R.O.,(1983) Near threshold fatigue crack propagation: A perspective on the role of crack closure. Proceedings of the conference on Fatigue Crack Growth Threshold Concept. AIME 227-261.
(16) Pook, L.P. (1988) The significance of mode I branch crack for mixed mode fatigue crack threshold behaviour. Biaxial and Multiaxial Fatigue, Mechanical Engineering Publications. 247-263.
(17) Erdogan, F. and Sih, G.C. (1963) On the crack extension in plates under plane loading and transverse shear. J. Basic Engng. Trans. ASME 85D, 519-527.

Table (1) Composition and Mechanical Properties of 316 Stainless Steel

Composition, wt.%

C	Mn	Si	S	P	Cr	Ni	Mo
0.049	1.36	0.54	0.018	0.023	17.26	11.20	2.15

Yield Stress (0.2% offset) N/mm^2	Tensile strength N/mm^2	Elongation %	Area Reduction %
246	595	67	66

Table 2 Precracking Histories for Two Specimens

B 11 with Load Shedding and B6 for Constant Load

Test No.	ΔK $MNm^{-3/2}$	Δa mm	da/dN nm/cycle
B.11	8.22	1.16	0.99
	8.06	0.38	1.06
	7.48	0.47	0.88
	7.11	0.27	0.66
	6.88	0.29	0.49
	6.21	0.19	0.35
	5.60	0.15	0.20
	5.15	0.10	0.19
B.6	7.50	0.90	0.99
	7.90	0.70	1.20
	8.20	0.80	2.10
	8.80	0.75	1.90
	9.00	0.82	2.00
	9.30	0.82	2.50

Table 3 Precracking Results

Test No.	Notch depth mm	a_o mm	ΔK_{Ith} $MNm^{-3/2}$	d_{ac} mm	R
B.1	9.02	14.34	4.71	1.99	0.1
B.2	9.08	15.38	4.60	2.10	0.1
B.3	9.02	15.58	5.25	3.00	0.1
B.4	8.94	16.06	6.0	1.82	0.1
B.7	8.81	14.51	4.47	3.41	0.1
B.8	8.72	15.19	4.56	3.63	0.1
B.9	9.09	15.70	5.12	3.50	0.1
B.10	8.27	13.36	5.10	2.64	0.5
B.11	8.92	11.93	5.15	1.00	0.5
B.12	8.70	13.28	4.75	1.50	0.5
B.13	9.94	14.75	4.96	2.35	0.5
B.14	8.66	14.62	4.71	2.20	0.5
B.5	9.01	10.40	9.26*	0	0.1
B.6	8.95	13.74	9.30*	0	0.1
A.10	9.82	11.16	10.96*	0	0.1

* Final K value applied

Table (4) Mixed Mode Test Results for R = 0.1

Test No.	B (mm)	W (mm)	a (mm)	a/W	So (mm)	P_{max} (kN)	P_{min} (kN)	ΔK_I ($MNm^{-3/2}$)	ΔK_{II} ($MNm^{-3/2}$)	$\frac{\Delta K_{II}}{\Delta K_I}$	$\frac{\Delta K_I}{\Delta Kth_I}$	$\frac{\Delta K_{II}}{\Delta Kth_I}$	θ_m	Comments
For Initial Coplanar Growth														
B2-1	15.20	30.06	15.25	0.50	0	17.70	1.77	0	4.06	∞	0	0.82		
B3-1	15.18	30.06	16.09	0.53	7.89	9.2	0.92	3.65	2.27	0.62	0.73	0.46		
B4-1	15.24	29.88	16.46	0.55	7.83	10.08	1.008	4.36	2.69	0.61	0.88	0.55		
B7-1	15.26	29.99	14.36	0.47	0	15.50	1.55	0	3.32	∞	0	0.67		
B8-1	14.96	30.06	15.16	0.50	2.61	6.66	0.66	1.45	2.65	2.05	0.29	0.53		
B9-1	14.95	30.03	15.70	0.52	4.52	14.45	1.44	3.43	3.66	1.06	0.69	0.73		
Non-Propagating (Coplanar Cracks)														
B2-2	15.20	30.06	15.30	0.50	0	28.70	2.87	0	6.56	∞	0	1.32		Δa = 0.05 mm
B3-2	15.18	30.06	16.21	0.53	7.89	12.0	1.20	4.93	3.03	0.61	0.99	0.61		Δa = 0.12 mm
B4-2	15.24	29.88	16.57	0.55	7.83	11.10	1.11	4.85	2.96	0.60	0.97	0.59		Δa = 0.11 mm
B7-2	15.26	29.99	14.41	0.47	0	42.77	4.27	0	8.89	∞	0	1.79		Δa = 0.05 mm by PD only
B8-2	14.96	30.06	15.20	0.50	2.61	31.4	3.14	3.93	7.31	1.86	0.79	1.47		Δa = 0.2 mm
B9-2	14.95	30.03	15.75	0.52	4.52	21.11	2.11	4.89	5.20	1.06	0.98	1.06		Δa = 0.05 mm
For Initial Branch Crack Growth														
B1-3	15.26	29.85	14.38	0.48	0	33.86	3.33	0	7.29	∞	0	1.47	-63	
B2-3	15.20	30.06	15.30		0	31.86	3.16	0	7.26	∞	0	1.46	-61	
B3-3	15.18	30.05	16.21	0.539	7.89	13.20	1.32	5.4	3.30	0.61	1.09	0.66	-40	
B4-3	15.24	29.88	16.57	0.554	7.83	13.0	1.30	5.63	3.43	0.60	1.13	0.69	-44	
B5-3	15.05	29.88	10.40	0.34	2.14	36.2	3.62	2.46	5.10	2.07	0.49	1.03	-63	
B6-3	15.27	30.14	13.76	0.45	8.31	13.33	1.33	4.57	2.86	0.62	0.92	0.57	-38	
B7-3	15.26	29.99	14.38	0.47	0	51.76	5.17	0	11.09	∞	0	2.24	-66	
B8-3	14.96	30.06	15.46	0.514	2.61	31.40	3.16	3.96	7.34	1.85	0.8	1.48	-49	
B9-3	14.95	30.03	15.75	0.524	4.52	24.12	2.41	5.53	5.77	1.04	1.11	1.16	-52	
A10	15.24	29.83	11.18	0.37	0	40.0	4.0	0	6.48	∞	0	1.30	-67	

Table (5) Mixed Mode Test Results for R = 0.5

Test No.	B (mm)	W (mm)	a (mm)	a/W	So (mm)	P_{max} (kN)	P_{min} (kN)	ΔK_I ($MNm^{-3/2}$)	ΔK_{II} ($MNm^{-3/2}$)	$\frac{\Delta K_{II}}{\Delta K_I}$	$\frac{\Delta K_I}{\Delta Kth_I}$	$\frac{\Delta K_{II}}{\Delta Kth_I}$	θ_m	Comments
For Initial Growth														
B10-1	15.03	29.98	13.38	0.44	5.57	17.68	8.84	2.22	1.94	0.87	0.45	0.394		
B11-1	15.0	29.83	11.93	0.39	13.1	15.24	7.62	3.98	1.41	0.35	0.80	0.28		
B12-1	15.05	30.06	13.28	0.44	1.93	40.0	20.0	1.68	4.26	2.53	0.34	0.86		
B13-1	15.24	29.83	14.75	0.49	0.55	54.0	27.0	0.80	6.87	8.58	0.16	1.39		
Non-Propagating Cracks														
B10-2	15.03	29.98	13.44	0.45	5.57	31.26	15.63	3.97	3.44	0.87	0.80	0.699		Δa = 0.06 mm
B11-2	15.0	29.83	11.97	0.40	13.11	18.59	9.29	4.80	1.74	0.36	0.97	0.35		Δa = 0.04 mm
B12-2	15.05	30.06	13.34	0.44	1.93	44.0	22.0	1.80	4.68	2.60	0.36	0.95		Δa = 0.06 mm
B13-2	15.24	29.83	14.88	0.49	0.55	54.0	27.0	0.93	7.63	8.58	0.18	1.74		Δa = 0.13 mm
For Initial Branch Crack Growth														
B10-3	15.03	29.98	13.44	0.45	5.57	37.81	18.90	4.78	4.16	0.87	0.97	0.84	-54	
B11-3	15.0	29.83	11.97	0.40	13.11	20.43	10.21	5.24	1.91	0.36	1.06	0.38	-40	
B12-3	15.05	30.06	13.34	0.44	1.93	51.90	25.83	2.24	5.66	2.52	0.45	1.15	-56	
B13-3	15.24	29.83	14.88	0.49	0.55	66.0	33.0	0.99	8.39	8.47	0.20	1.70	-61	
B14-3	15.24	30.11	14.69	0.49	0	72.0	36.0	0	7.57	∞	0	1.53	-75	

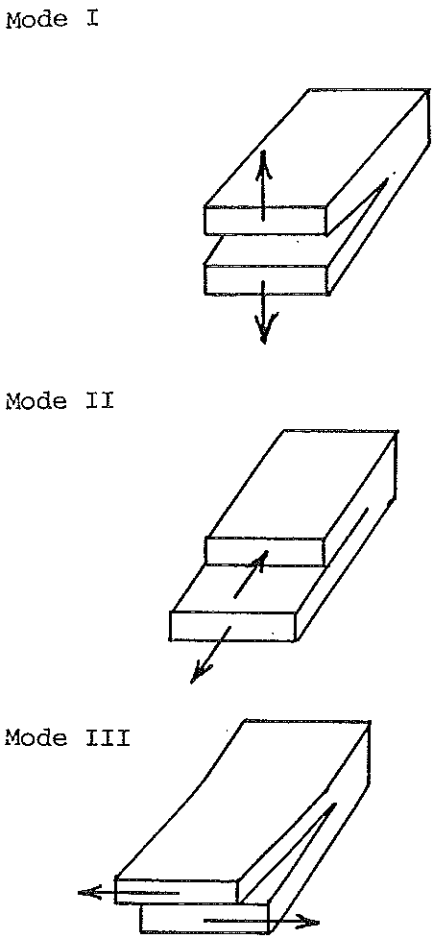

FIG. 1 Three modes of crack opening.

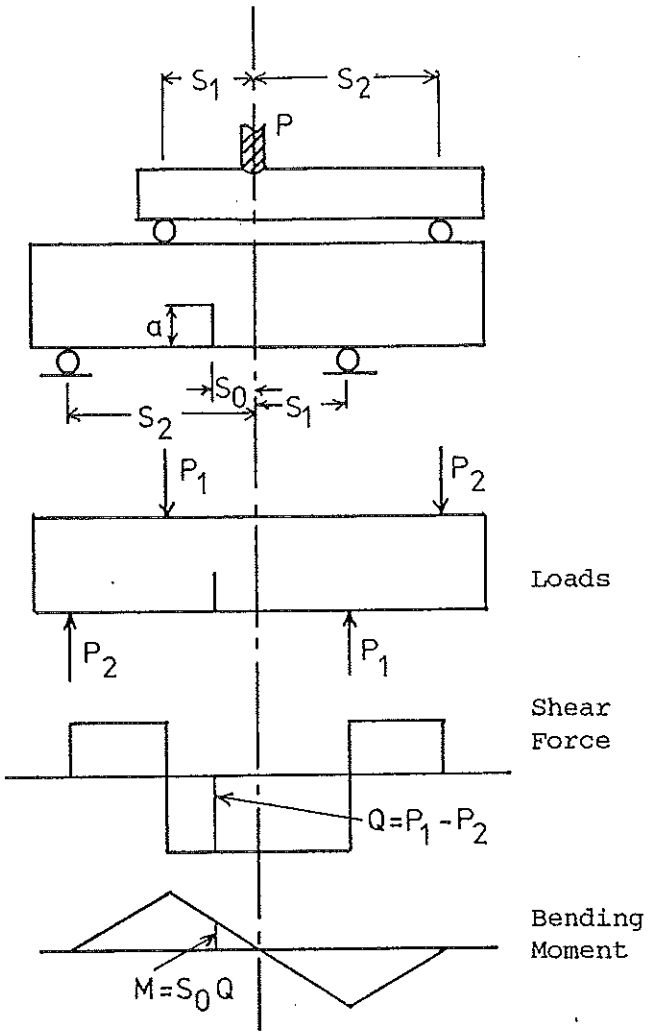

FIG. 2 Asymmetric four point bending.

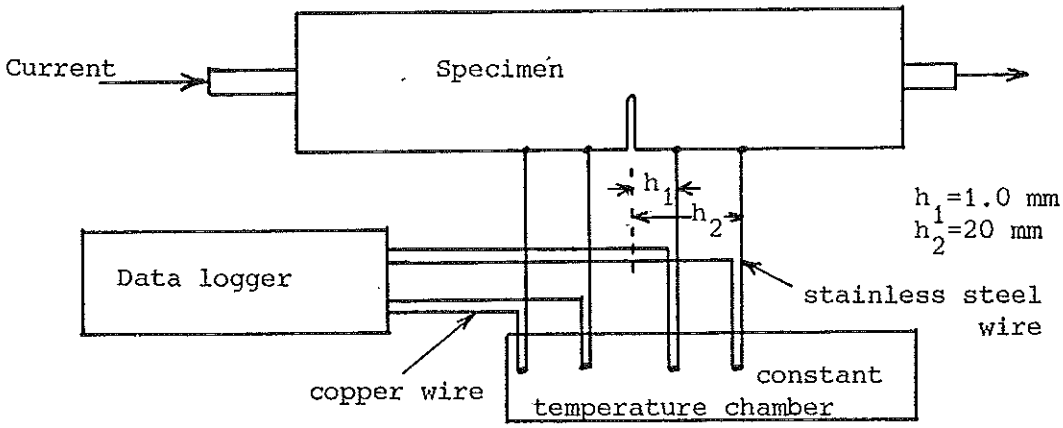

FIG. 3 Position of PD leads.

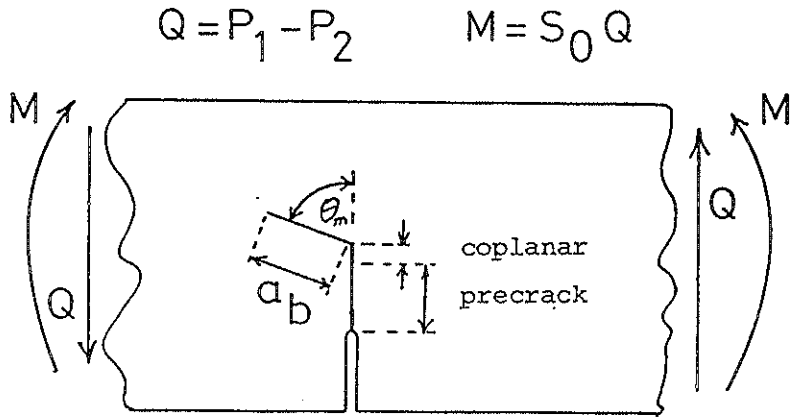

FIG. 4 Crack growth under mixed mode loading.

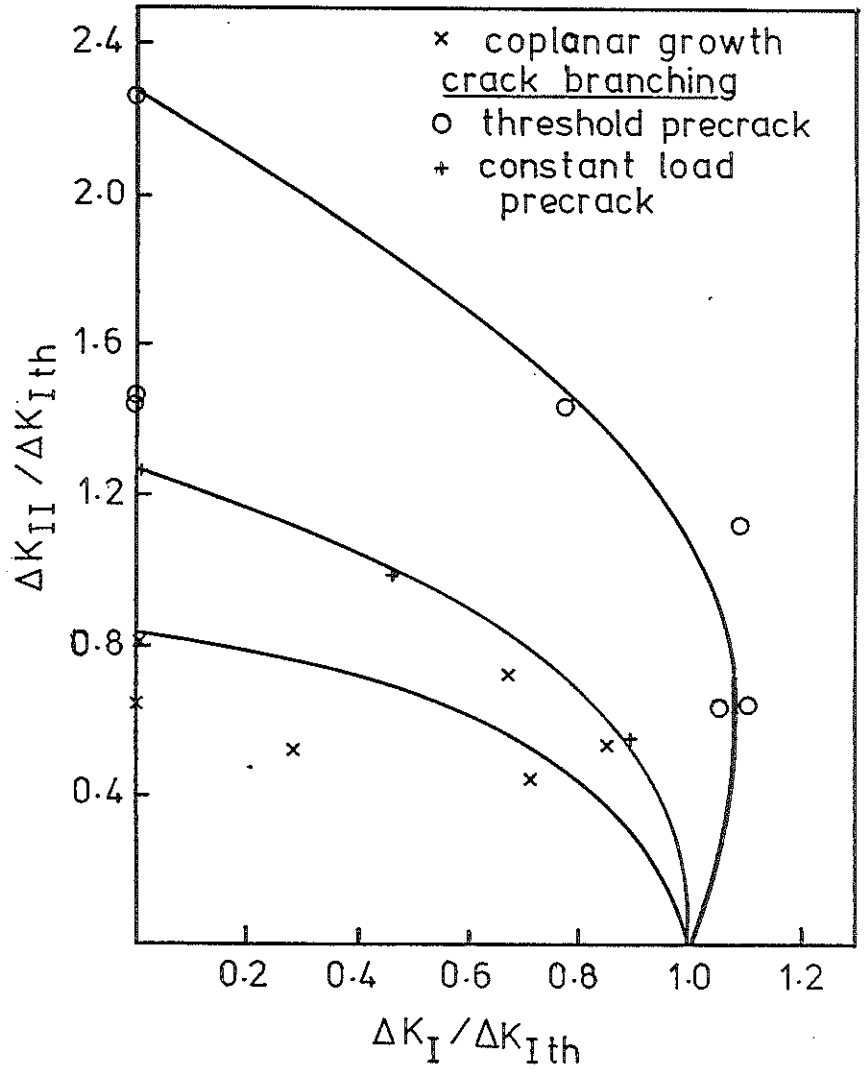

FIG. 5 Mixed mode thresholds for R = 0.1.

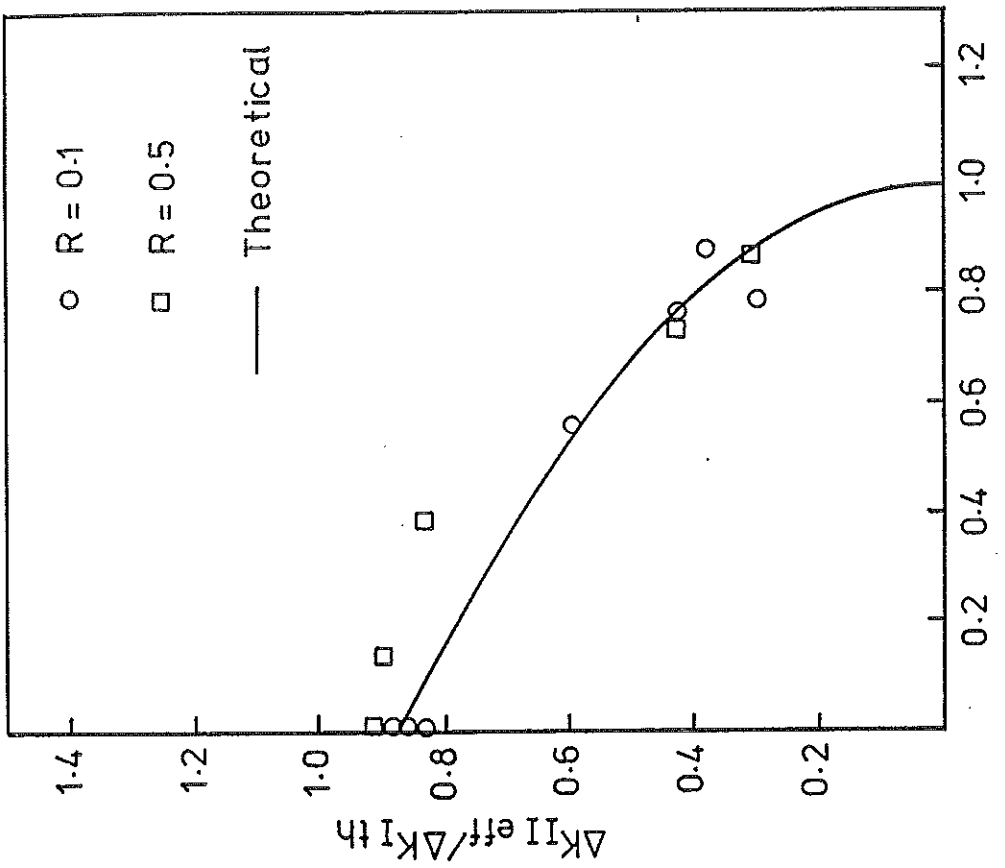

FIG. 7 Prediction of crack branching.

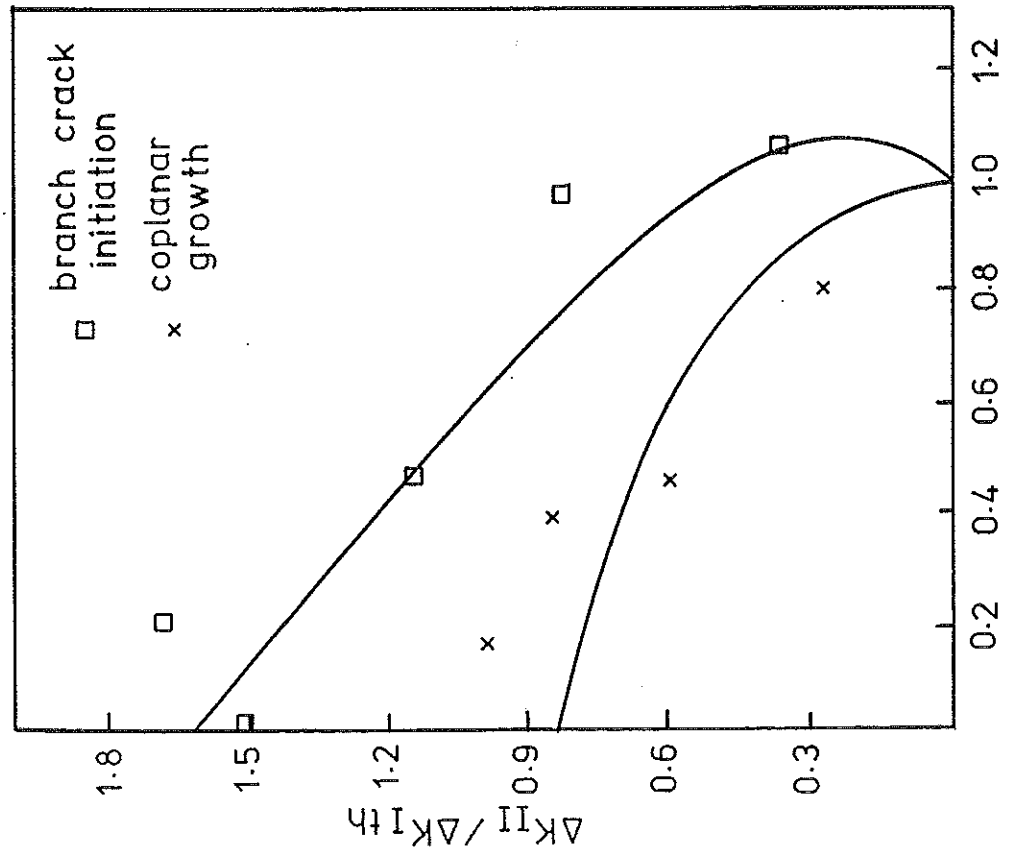

FIG. 6 Mixed mode thresholds for R = 0.5.

Fig. 8 Fracture surface for specimen B8, precracked down to threshold showing - 8(i) and 8(ii), region of rubbing behind the precrack tip and 8(iii) (a) branch crack, (b) coplanar growth, and (c) precrack.

Fig. 8(i)

1000 µm

Fig. 8(ii)

30 µm

Arrow indicated crack growth direction

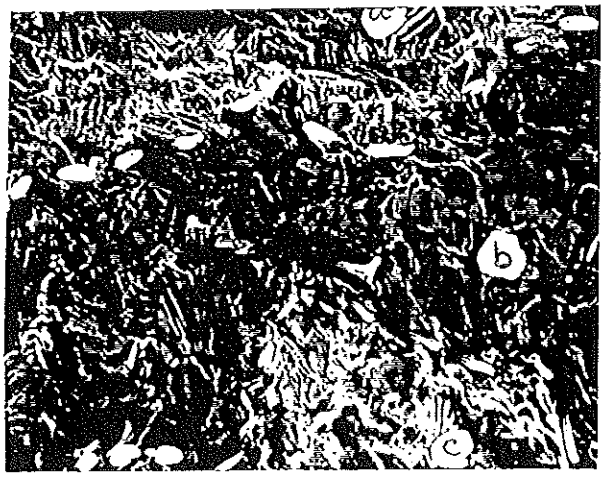

Fig. 8(iii)

100 µm

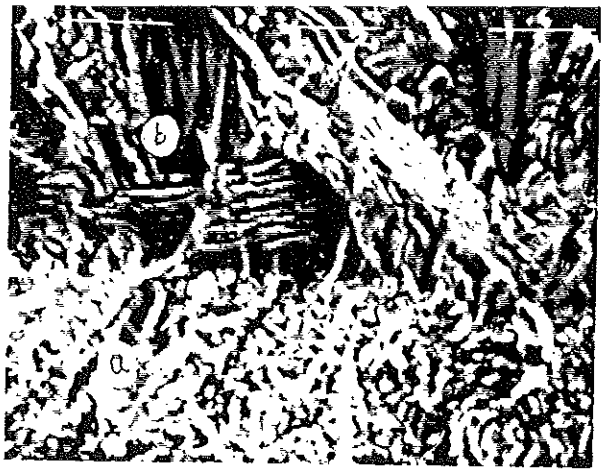

Fig. 9

10 µm

Fig. 9 Fracture surface for specimen B6, precracked at constant load, (a) precrack surface, (b) branch crack growth.

The Fatigue Crack Direction and Threshold Behaviour of a Medium Strength Structural Steel under Mixed Mode I and III Loading

L.P. Pook
D.G. Crawford

National Engineering Laboratory, Glasgow, UK